5-2009

Numerical Implementation of Prandtl's Lifting-Line Theory and Modeling of Aircraft Take-Off Phase for Wing Optimization

John William Dykes

Numerical Implementation of Prandtl's Lifting-Line Theory and Modeling of Aircraft Take-Off Phase for Wing Optimization

by

John W. Dykes

Undergraduate honors thesis under the direction of

Dr. Keith A. Gonthier

Department of Mechanical Engineering

Submitted to the LSU Honors College in partial fulfillment of
the Upper Division Honors Program.

May 2009

Louisiana State University
& Agricultural and Mechanical College
Baton Rouge, Louisiana

Abstract

The objective of the 2009 SAE Aero Design East competition was to design and build a remote-controlled, fixed-wing aircraft capable of carrying the heaviest possible payload through the required flight plan. Significant competition constraints include: a maximum allowable take-off distance of 200 feet, an unmodified O.S. MAX .61 FX engine, a material limitation prohibiting the use of carbon-fiber composites, and a size limitation restricting the aircraft's overall length, width, and height to 175 inches. From these constraints, the main wing was identified to be a critical component for the maximization of potential payload weight, and as a result, an optimization scheme was developed to determine the design of the wing. By modeling the aircraft take-off phase and enforcing the take-off distance to be approximately 200 feet, the maximum payload weight could then be determined for a wing shape of arbitrary wingspan, chord length, taper ratio, and airfoil profile. This take-off model accounts for the dynamics of the aircraft by using a modified form of *Newton's 2nd Law*, where the lift and drag forces acting on the main wing are determined through a separate aerodynamic model developed from *Prandtl's Lifting-Line Theory*. Utilizing these take-off and aerodynamic models, the optimization scheme yielded an overall design capable of carrying approximately 23 pounds of payload with a wing possessing a 96 inch wingspan, a constant chord length of 13.5 inches, and a GOE 226 airfoil profile.

Nomenclature

λ	Wing Taper Ratio
AR	Wing aspect ratio
b	Wingspan length
c	chord length
c_r	root chord length
c_t	tip chord length
S	Wing planform area
α	Angle of attack
α_{pitch}	Optimum angle for cruise flight
α_{eff}	Effective local angle of attack
α_i	Induced local angle of attack
$\alpha_{L=0}$	Zero-lift angle of attack
α_{stall}	Stall angle of attack
L'	2-D section lift
c_l	Section lift coefficient
c_d	Section drag coefficient
C_L	3-D wing lift coefficient
$C_{L\text{max}}$	Maximum 3-D lift coefficient
C_D	3-D wing drag coefficient
C_{Di}	3-D induced drag coefficient
C_{Do}	3-D Profile drag coefficient
Γ	Circulation
w	Downwash velocity
ρ	Air density
V_∞	Freestream velocity
$T(V)$	Thrust function
$L(V)$	Lift function
$N(V)$	normal force function
$f(V)$	Friction function
μ	Friction coefficient
$D(V)$	Drag function
g	Gravitational constant
m	Total aircraft mass
a	Aircraft acceleration
W	Total aircraft weight
W_{AC}	Unloaded aircraft weight
W_{PL}	Aircraft max payload weight
V_{stall}	Stall velocity
V_{TO}	Take-off velocity
S_{TO}	Take-off distance
S_G	Total ground roll distance
N	Even number of computational nodes
y	Wing Lifting-Line Coordinate Axis
y_0	Particular y-location on wing
Γ_0	Initial Γ profile parameter
F_i	Shorthand numerical integrand

Contents

List of Figures

1 Introduction

The SAE Aero Design® is an international collegiate competition designed to introduce students to real-life engineering challenges in an aerospace related setting. Within this competition, dozens of teams, each comprised of several engineering students under the supervision of one faculty advisor, compete to design, build, and fly a unique remote controlled model aircraft capable of carrying the heaviest payload possible. Several different classes exist for students to compete in, each with their own specific design constraints and objectives. The one commonality between each class is that the students are solely responsible for the formulation of a unique design solution that is optimized for the challenge at hand. Within the design phase of the competition, several important aerospace related topics are addressed including aerodynamics and optimization, flight dynamics, and flight controls. Also, students are encouraged to explore the use of new and innovative construction techniques and materials within their designs in an effort to help spur creativity and interest among the scientific community.

1.1 Competition Constraints and Objectives

The primary objective of the SAE Aero Design® competition is to design and build a unique remote controlled aircraft capable of lifting as much weight as possible while still observing the preset motor and size constraints. For the regular class, the aircraft must be capable of carrying a 5 in.x 5 in.x 10 in. rectangular block (payload) of which the design team is responsible for making as heavy as possible. Extra emphasis is placed on the ability of the design team to accurately predict the maximum payload carrying capacity of their aircraft. Additionally, the aircraft must not possess a combined overall length, width, and height measurement greater than 175 inches. The power requirement for the regular class is an unmodified O.S. MAX .61 FX with stock muffler.[1]

In addition to certain design objectives and constraints imposed by contest regulations, the aircraft must be able to maintain stable and controlled flight while being remotely piloted by one of the team members. Once the payload is attached to the airframe, the pilot must fly the aircraft through a strict flight plan consisting of three primary objectives:

- Take-off from rest within 200 feet
- Complete on 360° circuit of the flight area without crossing into the *No-Fly Zones*
- Land on the runway within the 400 foot landing zone. Figure 1 illustrates the flight plan layout at the competition.

Recently, the design competition has restricted the use of any carbon fiber or glass composites on the aircraft. This greatly increases the importance of both the aerodynamic and structural analyses, because "thin-airfoiled" wings are no longer a viable design option.

[1] 2-Stroke, internal combustion engine; 0.61 cubic inch displacement

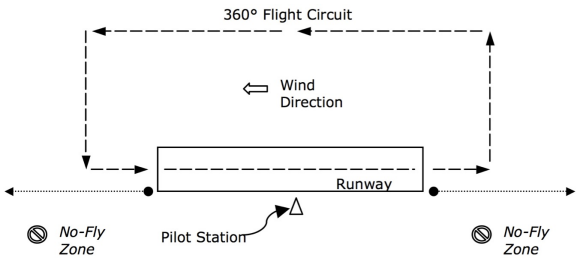

Figure 1: Flight plan layout and field orientation.

1.2 Wing Design Methodology

From the competition constraints and objectives, several analyses were identified for addressing critical issues. In the case of the main wing an analysis was required for the determination and selection of various geometric parameters in order to maximize the payload weight. In order to achieve this two different phases of the flight plan were investigated: (1) the cruise flight phase and (2) the take-off phase. Priority was given to the take-off phase, since optimizing for cruise flight suggests that the aircraft range is sought to be maximized per amount of fuel. This of course is not a critical factor in this case due to the flight plan being both simple and brief.

The design was based on a high-wing cargo plane type configuration with initial dimensions determined from aircraft design spreadsheets from Corke [2]. This provided only a starting point, however, due to scaling inaccuracies with RC size aircraft. Therefore the dimensional parameters given by these spreadsheets were taken as "ballpark estimates" and ultimately used as initial guesses for an optimization algorithm on the wing. The goal of this algorithm (see Figure 2) was to enforce the competition constraints so that at least a local optimum wing design could be determined. Implementation of this algorithm required the development of two models: (1) an aerodynamic model and (2) a take-off model.

The primary function of the aerodynamic model was to evaluate lift and drag on a given wing shape as a function of both flight velocity and the ambient conditions. This data may then be used by the take-off model to determine payload weight based on the allowable take-off distance.

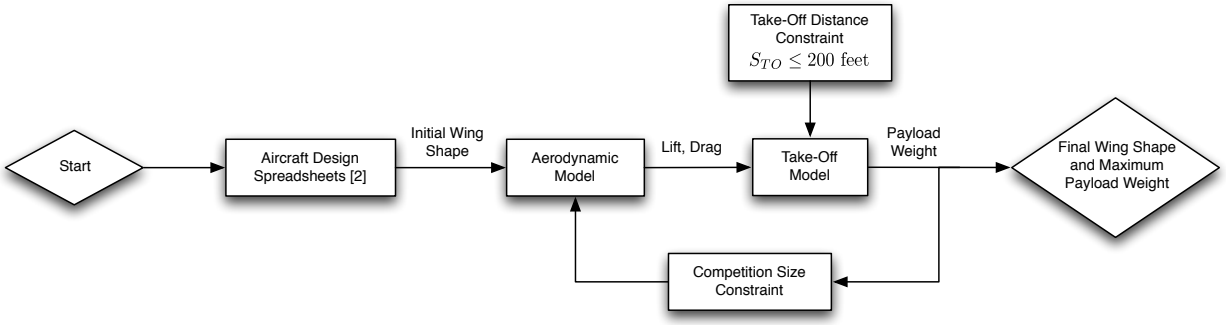

Figure 2: Wing Optimizer Algorithm

In order to accurately model both the aerodynamic forces and the take-off phase, mathematical models must first be developed based on theory and then properly implemented using numerical techniques. The next sections derive the methods used for development of both models. Uninterested or knowledgeable readers are advised to skip ahead to section 2.2 to retain continuity.

2 Aerodynamic Model

2.1 Background & Theory

The selected aerodynamic model was based on an incompressible, inviscid flow analysis for finite wings, formally known as *Prandtl's Classical Lifting-Line Theory*. Developed during World War I by Ludwig Prandtl, this theory provided the first practical model for analyzing finite wings and is still in use today for preliminary wing analysis [3]. A model implementing this theory is capable of evaluating aerodynamics forces (*i.e. Lift and Drag*), assuming that both the wing geometry and the 2D airfoil data are known. Therefore in order to derive and construct a relevant model, it is necessary to start by introducing the appropriate terminology for finite wing and airfoil sections.

2.1.1 Wings & Airfoils

Airfoil sections are defined as two-dimensional structures with curved, streamlined surfaces designed to give the most favorable lift to drag ratio in flight. Airfoils are used as the most basic from of an aircraft wing as well as many other applications such as windmills, race cars, submarines, etc. In fact, for the general concept of extracting energy from any moving fluid requires the use of airfoil shaped surfaces. A general airfoil shape is shown in Figure 3(a).

Figure 3(b) illustrates a planform (or top) view of a linearly tapered finite wing. The variables c_r and c_t represent the airfoil chord lengths at the wing root and tip. For an arbitrary wing, any point along the wing span b corresponds to an arbitrarily shaped airfoil with chord length c. Considering the previous statement, a wing may also be thought of as a stack of thinly sliced airfoils with corresponding chord length. This concept will prove to be useful subsequently in the numerical implementation sections.

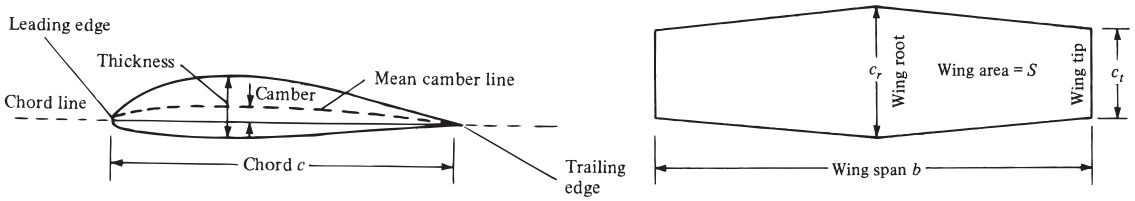

Figure 3: (a) Generic airfoil profile with standard nomenclature and (b) planform view of a linearly tapered aircraft wing with relevant parameters defined [3].

In addition to the parameters previously defined for wing, two dimensionless parameters provide insight into the geometry of the wing: the aspect ratio AR and taper ratio λ. Starting with the taper ratio, it may be defined as follows.

$$\lambda = \frac{c_t}{c_r} \tag{1}$$

Perhaps the most useful wing parameter is the aspect ratio defined below.

$$AR = \frac{b^2}{S} \tag{2}$$

The aspect ratio describes how long and slender or short and fat the wing is. Typically in design, this parameter is desired to be maximized to its practical limit. This is because, aerodynamically speaking, the lift to drag ratio is increased as the aspect ratio becomes very large [3]. This is usually limited due to structural limitations; however, in context to the competition the size constraint will prove to be a limiting factor with this parameter. Based on the previous expressions, a complete wing design may be set by determining four parameters: (i) aspect ratio, AR; (ii) planform area, S; (iii) taper ratio, λ; and (iv) airfoil profile. Other parameters such as wing sweep and dihedral were not considered in this design.

2.1.2 General Airfoil Lift Characteristics

For an airfoil to produce lift[2], the profile should be non-symmetrical about the chord line (*i.e.* possess chamber) or the leading edge should be directed into the flow, where angle between the chord line and the incoming flow should be relatively small. This angle is defined as the airfoil's angle of attack, α, and is positive in the clockwise (or pitch-up) direction. Figure 4 shows a general normalized[3] lift curve as a function of the angle of attack.

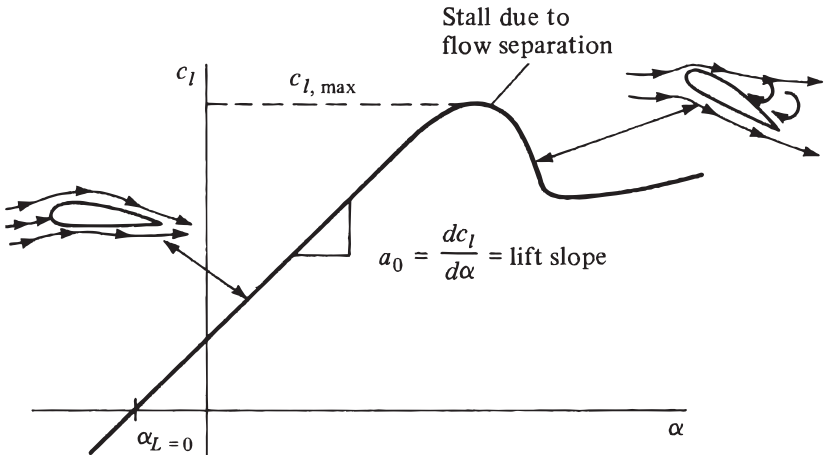

Figure 4: Typical $c_l(\alpha)$ curve for a cambered airfoil [3].

[2]Lift for an airfoil is actually section lift (per unit span), designated L', since it is purely two-dimensional.
[3]Normalized section lift is defined as $c_l = L'/q_\infty c$, where $q_\infty = \frac{1}{2}\rho U^2$ and c is the chord length.

This trend provides critical insight into the behavior of efficient lifting airfoil shapes. Notice that a large portion of the lift curve is linear. This suggests that the lift slope $dc_l(\alpha)/d\alpha$ is equal to a constant value[4]. The value $\alpha_{L=0}$ is the angle of attack at which the airfoil produces zero-lift and is a strong function of the airfoil chamber. If an airfoil does not possess any chamber then this value will be $\alpha_{L=0} = 0°$. The range of lift coefficients spanning from $\alpha_{L=0}$ to a corresponding angle at the maximum lift coefficient $c_{l_{\max}}$ is known as the stall margin and is the range where most aircraft commonly operate at during flight.

Qualitatively, airfoils are able to produce lift because of an induced pressure gradient along the airfoil surface that is favorable to lift. Throughout the stall margin, this lift is a linear function of angle of attack as previously mentioned, but at angles above α_{stall} this is no longer valid due of flow separation from the upper surface.

2.1.3 Potential Flow Theory

A quantitative analysis known as *Potential Flow Theory* is commonly used for determining the lift characteristics of low-speed flows over airfoils. This theory is valid so long as the flow around the airfoil is (1) *incompressible* and (2) *inviscid*. This means that both the density changes and the frictional effects of the air flow around the airfoil are neglected. Mathematically, it can be shown by *Conservation of Mass* for an incompressible continuum that the velocity field must satisfy the following expression.

$$\vec{\nabla} \cdot \vec{V} = 0 \tag{3}$$

Similarly, performing a *Momentum Conservation* analysis on a potential flow results in the well known *Bernoulli Equation*. This relation has the ability to relate the pressure and velocity at any point in the flow field to another, as shown below.

$$P_1 + \frac{V_1^2}{2} + \rho g h_1 = P_2 + \frac{V_2^2}{2} + \rho g h_2 \tag{4}$$

For this equation, the effects of gravity may be neglected since the density of air is small. Unfortunately, the above two expressions are still incomplete to accurately govern the lift forces on an airfoil. This is because, by neglecting friction, we have enforced the constraint that the flow also be what is called *irrotational*. The mathematical representation of this result is shown below.

$$\vec{\nabla} \times \vec{V} = 0 \tag{5}$$

This expression[5] leads to the unfavorable result that a body cannot produce lift without the presence of friction [3]. Therefore further investigation must be performed to determine an applicable concept of lift from Eq. (5).

[4]From thin-airfoil theory, $dc_l/d\alpha \approx 2\pi$ for airfoils with moderate thickness[2].

[5]$\vec{\nabla} \times \vec{V}$ is sometimes referred to as vorticity, denoted by the symbol $\vec{\xi}$.

2.1.4 Circulation & Lift

Lord Kelvin's Circulation Theorem ultimately resolved the issue of how to approach the concept of conserving rotation within the fluid such that vorticty may locally exist around the airfoil. This was done by introducing the concept of a "*starting vortex*" of equal strength and opposite rotation to that of an airfoil such that the net rotation of the fluid still satisfies Eq. (5). This was achieved by utilizing the concept of vortex strength called *circulation*. This mathematically represents the integral contributions of a rotational fluid over an area, as summarized by the integral below.

$$\Gamma = -\iint_S (\vec{\nabla} \times \vec{V}) \cdot \hat{n} \; dS \tag{6}$$

By application of *Stoke's Theorem* from multivariable calculus, the circulation may also be expressed as a line integral.

$$\Gamma = -\oint_A \vec{V} \cdot d\vec{s} \tag{7}$$

Ultimately, the circulation was able to be related to the section lift an airfoil by the *Kutta-Joukowski Theorem*, which was developed in the early 20th century [3]. Perhaps the most important relation in aerodynamics, this fundamental theorem states that the circulation is directly proportional to the lift as shown below.

$$L' = \rho_\infty V_\infty \Gamma \tag{8}$$

This is an extremely powerful result because it states that the velocity may be integrated around any arbitrarily-shaped control volume to solve for the total airfoil lift. Figure 5 illustrates these concepts, where the dashed line represents the boundary of an arbitrary control volume.

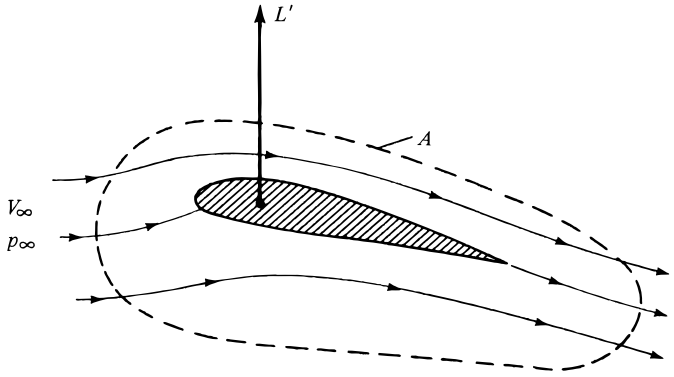

Figure 5: Circulation around any arbitrarily-shaped control surface can be related to the section lift by the *Kutta-Joukowski Theorem* [3].

2.1.5 Airfoil Theories

Based on the previous discussions, the lift curve for an airfoil may now be found through development airfoil theories. The classical *Thin Airfoil Theory* was developed by replacing the chamber line of an airfoil with a "sheet" of vortex filaments, which are simply lines of constant vorticity. By assuming that the airfoil is (1) infinitely thin and (2) the flow field cannot cross the surface of the chamber line, the vortex filaments may be analytically solved for and related to the lift via the *Kutta-Joukowski Theorem*. One useful result of this theory was the claim that the lift slope in the stall margin was linearly proportional to angle of attack by 2π radians, which very nearly approximates the general trend outlined in Figure 4. Additionally, methods exist for evaluating airfoils with thickness utilize numerical vortex-panel approximations.

One significant shortcoming of these theories, however, is the inability to predict the stall characteristics such as α_{stall} and $c_{l_{\max}}$. Physically, this is because viscous forces dominate causing flow separation and wake formation. Therefore the assumption of an inviscid fluid is no longer valid at this point. Even so, airfoil theory does a good job of predicting lift behavior throughout the stall margin. For this application, the open-source potential flow solver *XFOIL* [5] embedded in the *Profili* [6] airfoil library, which provided airfoil lift, drag, and quarter-chord pitching moment data.

2.1.6 Finite Wing Theory

Another way of considering the previously discussed airfoil theory is to imagine a wing with infinite span and constant lift distribution. For a finite wing, however, this is not the case. Instead, an aerodynamic effect known as *downwash* results in a varying lift distribution that approaches a value of zero at the wing tips. This is a direct result of the tendency for the high pressure air flowing underneath the wing to move around the wing tips to the lower pressure flow on the upper surface. This phenomenon, being dependent on the pressure ratio across both sides of the wing, is therefore highly dependent on the lift. For this reason, the tip effects are commonly referred to as being "*lift-induced*". The figure below shows an example of how finite wings induce tip vortices that both detract from the lift and contribute to the drag. This component of the wing drag is referred to as *induced drag* and can account for up to 60% of the drag [4].

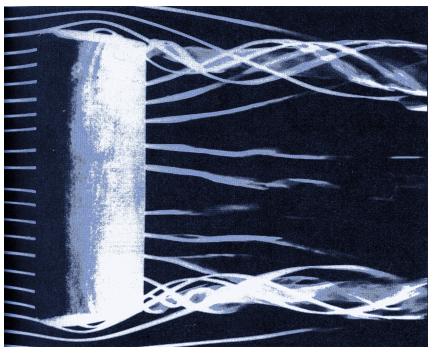

Figure 6: Flow visualization of lift-induced tip effects on a finite wing [3].

Induced drag is due to the downwash velocity w caused by the tip effects. As a result, this downwash slightly adjusts the of the freestream velocity vector at local airfoil sections along the wing. Revisiting the concept considering a finite wing to be a stack of thinly sliced airfoils, the previous statement implies that each individual airfoil feels its own unique "effective" angle of attack α_{eff}. The value of this angle is the difference between the known global angle of attack of the wing α and the induced angle of attack α_i . As shown in figure below, α_i can be derived from trigonometric relationships.

$$\alpha_i(y_0) = \arctan\left(-\frac{w(y_0)}{V_\infty}\right) \approx -\frac{w(y_0)}{V_\infty} \tag{9}$$

This angle is important because if α_i is known then α_{eff} is also known, and thus, the corresponding section lift may be found from the airfoil lift curve. Therefore the key to quantifying the lift distribution over the span of a finite wing is to derive a suitable expression for the downwash velocity w.

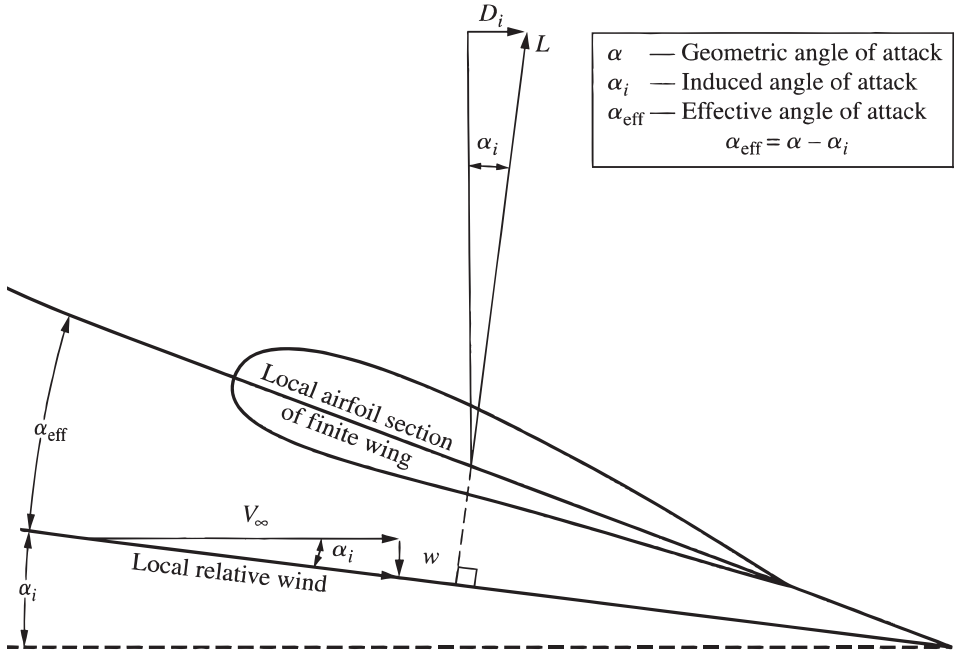

Figure 7: A cross-section of an airfoil section of a wing with the lift-induced components of downwash diagramed [3].

2.1.7 Prandtl's Lifting-Line Theory

This theory is based on the two basic principles of vortex behavior postulated by the German methematician *Hermon von Helmholtz*. According to Helmholtz's vortex theorems [3], (1) the strength of a vortex filament is constant along its length, and (2) a vortex filament cannot end in a fluid. This knowledge allowed Prandtl develop the concepts of *bound* and *free* vortices, which ultimately led to modeling a finite wing with a *horseshoe vortex*.

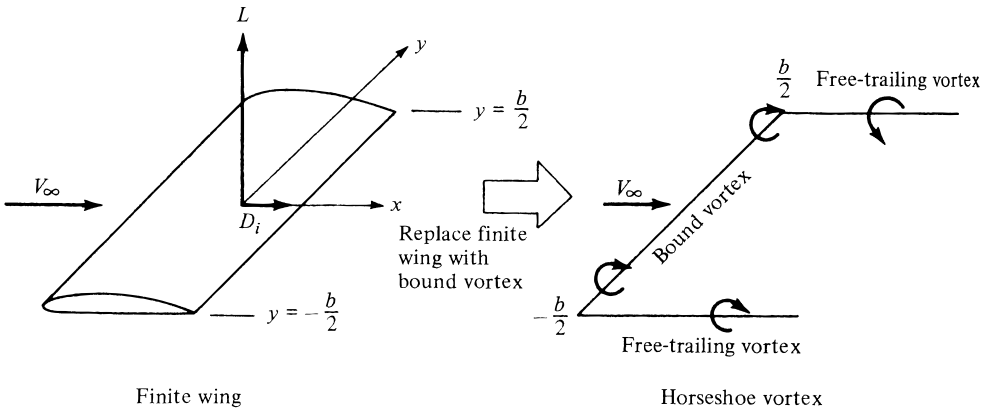

Figure 8: *Prandtl's Lifting-Line Theory* models the finite wing as a conceptual horseshoe vortex [3].

From the figure above, it is observed that the bound vortex represents the finite wing and the two free vortices represent the wing tip effects. Utilization of the *Biot-Savart Law*, commonly found in electro-magnetism physics, results in the following expression for the downwash distribution $w(y)$ over the bound vortex [3].

$$w(y) = -\frac{\Gamma}{4\pi}\frac{b}{(b/2)^2 - y^2}. \tag{10}$$

Unfortunately, the equation above is not useful for ultimately determining the lift distribution across the wing due to the nonphysical result of approaching $-\infty$ at the wing tips. Figure 9 illustrates this fact.

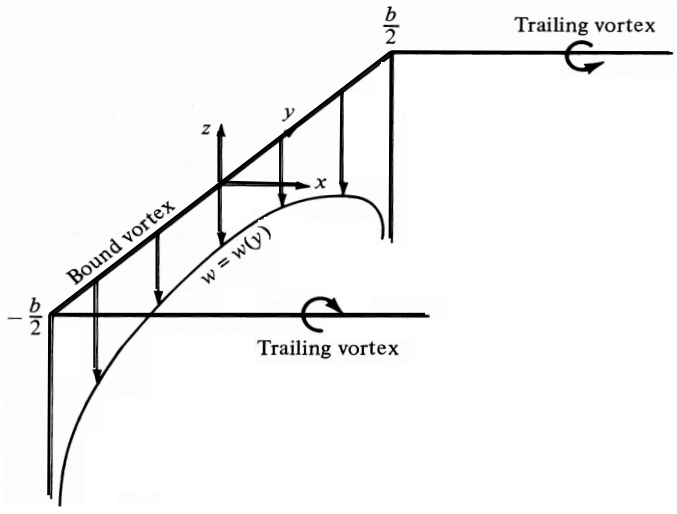

Figure 9: An illustration of the derived downwash distribution of Eq. (10) over the bound vortex (of finite wing) which is ill-behaved at $\pm b/2$ [3].

Prandtl ultimately solved this problem by superimposing a large number of horseshoe vortices, as upposed to modeling a wing with a single horseshoe vortex filament. Illustrated in Figure 10, this superposition method implies that each horseshoe vortex (1) has a different bound vortex filament length as well as (2) its own unique value of differential strength $d\Gamma_i$. Now, application of the *Biot-Savart Law* for a differential downwash element at an arbitrary point y_0 on the wing span yields the following result.

$$dw(y_0) = -\frac{d\Gamma}{4\pi(y_0 - y)} = -\frac{d\Gamma/dy}{4\pi(y_0 - y)}\, dy. \tag{11}$$

Finally, the downwash distribution along the wingspan may be found through integration, which correctly approaches a finite value resulting in zero lift at $\pm b/2$ as anticipated.

$$w(y_0) = -\frac{1}{4\pi}\int_{-b/2}^{b/2} \frac{d\Gamma/dy}{y_0 - y}\, dy. \tag{12}$$

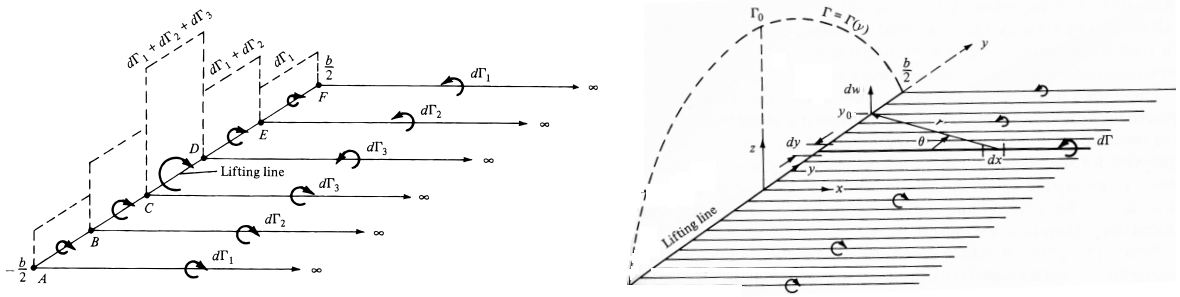

(a) (b)

Figure 10: (a) A superposition of a small finite number of horseshoe vortices results in a low resolution distribution while (b) a very large number of horseshoe begins more accurately model tip effects [3].

Now that the amount of downwash can be quantified, the induced angle of attack α_i may easily be found via Eq. (9).

$$\alpha_i(y_0) = \frac{1}{4\pi V_\infty}\int_{-b/2}^{b/2} \frac{d\Gamma/dy}{y_0 - y}\, dy. \tag{13}$$

Since $\alpha_{\text{eff}}(y_0) = \alpha - \alpha_i(y_0)$ (from Figure 7), *the fundamental equation of Prandtl's lifting-line theory* may ultimately be derived and expressed in the following Eq. (2).

$$\boxed{\alpha(y_0) = \frac{\Gamma(y_0)}{\pi V_\infty c(y_0)} + \alpha_{L=0} + \frac{1}{4\pi V_\infty}\int_{-b/2}^{b/2} \frac{d\Gamma/dy}{y_0 - y}\, dy} \tag{14}$$

This expression is a complicated nonlinear integro-differential equation; however, the only unknown for a given wing design and operation is the circulation distribution $\Gamma(y_0)$. If the

circulation distribution were able to be solved for then the *Kutta-Joukowski Theorem* may be utilized to easily determine the lift distribution.

$$L'(y) = \rho_\infty V_\infty \Gamma(y) \tag{15}$$

Similarly, the induced drag distribution can be solved for based off the diagram in Figure 7.

$$D_i'(y) = L'(y) sin(\alpha_i) \tag{16}$$

To find the total contribution of these forces on the wing requires simple integration over the span. Since it is often desirable to normalize these parameters by dynamic head q_∞ and planform area S, the two equations below are displayed as the total lift and induced drag coefficients over a wing.

$$C_L = \frac{L}{q_\infty S} = \frac{2}{V_\infty S}\int_{-b/2}^{b/2} \Gamma(y) dy \tag{17}$$

$$C_{D_i} = \frac{D_i}{q_\infty S} = \frac{2}{V_\infty S}\int_{-b/2}^{b/2} \Gamma(y) sin(\alpha_i)\, dy \tag{18}$$

From Eq. (17) and Eq. (18), the power of the lifting-line theory can be realized through use of the Kutta-Joukowski Theorem. Simply put, if the circulation distribution in Eq.14 can be solved for then the aerodynamic forces, lift and induced drag, can be completely described.

2.2 Numerical Implementation of the Lifting-Line Method

Prandtl's lifting-line theory cannot be analytically solved for $\Gamma(y)$ because of the nonlinear nature of Eq. (14). Thus, a numerical model was created that utilizes an iterative method to converge on an approximate solution [4]. In order to achieve this both the integral of Eq. (13) and the differential circulation $d\Gamma/dy$ inside that integral will need to be numerically approximated.

The first step in developing this model is to discretize the wing span into $N+1$ evenly spaced nodes, where N is an even number, as illustrated in Figure 11. The odd nodes are denoted by a filled circle, while even nodes are denoted by an open circle. The nodes are "staggered" in order to avoid numerical complications. $\Gamma(y_j)$ and $\alpha_i(y_j)$ will be computed on the odd nodes, while the integrals in $\alpha_i(y_j)$ Eq. (13) will be calculated along the even nodes.

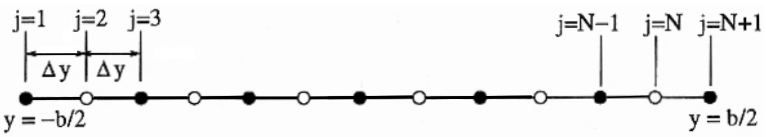

Figure 11: Numerical representation of a wing span where each nodes corresponds to an airfoil shape and position [4].

Next, an initial guess for $\Gamma(y)$ must be supplied as a starting point for the convergence loop. The expression below was used for this initial guess, where the only value to be provided for this initial guess is the maximum circulation value Γ_0.

$$\Gamma(y) = \Gamma_0 \sqrt{1 - \left(\frac{y_j}{b/2}\right)^2} \tag{19}$$

Before the integral expression for α_i may be evaluated, the values of $d\Gamma/dy$ inside the integral will need to be numerically approximated along the even nodes. Using what is referred to as a second-order accurate finite difference approximation the following relationship holds.

$$\left(\frac{d\Gamma}{dy}\right)_k \approx \frac{\Gamma(y_{k+1}) - \Gamma(y_{k-1})}{2\Delta y} \tag{20}$$

Therefore the numerical approximation of the entire integrand may now be represented.

$$F_k \approx \frac{(d\Gamma/dy)_k}{y_j - y_k} \tag{21}$$

From Eq. (21), it now becomes apparent why alternating nodes must be done because, otherwise, a singularity point will be present (*i.e.* $y_j - y_k = 0$) and the integral will not be well behaved at that point. The integral in Eq. (13) may now be approximated over only the even nodes using *Simpson's 1/3 rule*.

$$\int_{y_2}^{y_N} \frac{d\Gamma/dy}{y_j - y}\, dy \approx \Delta y \left(F_2 + F_N + 2 \sum_{k=4,6,8\ldots}^{N-2} F_k \right) \tag{22}$$

Contributions to the integral from the left and right most intervals can be approximated by:

$$\int_{y_1}^{y_2} \frac{d\Gamma/dy}{y_j - y}\, dy \approx \frac{\Delta y}{2}\left(F_1 + F_2\right) \tag{23}$$

$$\int_{y_N}^{y_{N+1}} \frac{d\Gamma/dy}{y_j - y}\, dy \approx \frac{\Delta y}{2}\left(F_N + F_{N+1}\right) \tag{24}$$

Here, F_1 and F_{N+1} can be loosely guesstimated by first-order Taylor series expansions.

$$F_1 \approx \frac{3F_2 - F_4}{2} \tag{25}$$

$$F_{N+1} \approx \frac{3F_N - F_{N-2}}{2} \tag{26}$$

Generally speaking, extrapolating values in numerical methods is a recipe for ill-behaved solutions. In this case the number of nodes N will be chosen to be considerably high such that the error in these equations is relatively small.

Now having numerically evaluated Eq. (13) for every $\alpha_i(y_j)$ along the wing span, corresponding values of $\alpha_{\text{eff}}(y_j)$ may be found and used to find the local section lift coefficient

data $c_l(y_j)$ at each node given that the 2-D airfoil lift coefficient as a function of α_{eff} is known. This $c_l(y_j)$ may now be used in a modified form of the Kutta-Joukowski Theorem to determine a new distribution of circulation $\Gamma_{\text{new}}(y)$.

$$\Gamma_{\text{new}}(y) = \frac{1}{2} V_\infty c(y_j) c_l(y_j) \tag{27}$$

The term $c(y_j)$ represents the chord length at point y_j, which is allowed to linearly vary for a given taper ratio λ.

Using Γ_{new}, convergence can be checked by taking $d_j = |\Gamma_{\text{new}} - \Gamma_{old}|$ for each node j and then finding $||\vec{d}||$. If not yet converged, then the circulation distribution must be updated using the equation below for each j.

$$\Gamma_{\text{input}} = \Gamma_{\text{old}} + D(\Gamma_{\text{new}} - \Gamma_{\text{old}}) \tag{28}$$

D is a convergence damping parameter approximately ranging in value from $D \approx 0.01$-0.05. It is also necessary for each iteration must impose $\Gamma_1 = \Gamma_{N+1} = 0$ for proper convergence so as to not yield nonphysical results. For this study, the convergence was defined for $||\vec{d}|| \leq 10e^{-8}$.

Once convergence has been obtain, the final values of $\Gamma(y)$ may now be used to obtain the lift distribution $L'(y)$ or the total lift coefficient C_L Eq. (17). Again, Simpson's 1/3 rule may be used to approximate integration.

$$C_L \approx \frac{2\Delta y}{V_\infty b} \left[\frac{\Gamma(y_1)}{c(y_1)} + \frac{\Gamma(y_{N+1})}{c(y_{N+1})} + 2 \sum_{k=3,5,7\ldots}^{N-1} \frac{\Gamma(y_k)}{c(y_k)} \right] \tag{29}$$

Likewise, the induced drag can be approximated.

$$C_{D_i} \approx \frac{2\Delta y}{V_\infty b} \left[\frac{\Gamma(y_1)}{c(y_1)} \sin\, \alpha_i(y_1) + \frac{\Gamma(y_{N+1})}{c(y_{N+1})} \sin\, \alpha_i(y_{N+1}) + 2 \sum_{k=3,5,7\ldots}^{N-1} \frac{\Gamma(y_k)}{c(y_k)} \sin\, \alpha_i(y_k) \right] \tag{30}$$

While the induced drag is a major component of drag on the a, it does not account for the affects of skin friction drag and pressure drag. Often these two types of drag are referred to collectively as profile drag C_{D_o}. This profile drag was also able to be numerically accounted for by utilizing the results of the lifting-line model and 2-D airfoil drag data[6] provided by *XFOIL* and *Profili*. Using the final values for $\alpha_{\text{eff}}(y_j)$, the section drag distribution $D'_\text{o}(y_j)$ was found.

$$D'_\text{o}(y_j) = q_\infty c(y_j) c_d(y_j) \tag{31}$$

Now the wing drag coefficient may be determined through integration and approximated as follows via Simpson's 1/3 rule.

$$C_{D_\text{o}} = \frac{2\Delta y}{q_\infty b} \left[\frac{D'_\text{o}(y_1)}{c(y_1)} + \frac{D'_\text{o}(y_{N+1})}{c(y_{N+1})} + 2 \sum_{k=3,5,7\ldots}^{N-1} \frac{D'_\text{o}(y_k)}{c(y_k)} \right] \tag{32}$$

The total drag on a wing is finally found with the summation of Eq. (30) and Eq. (33).

$$C_D = C_{D_i} + C_{D_\text{o}} \tag{33}$$

[6]Also the airfoil quarter-chord moment data was used to find the pitching moment C_M for use in both stability and stress analyses. These analyses are not discussed in this report; however, a sample output of this data and corresponding Matlab code can be seen in the Appendix D.

2.3 Lifting-Line (Aerodynamic) Model Sample Output

As previously mentioned, the lifting-line method allows for the complete determination of aerodynamic forces acting on an arbitrarily shaped wing. Referring back to the optimizer flowchart (Figure 2 of section 1.2), the lift and drag forces acting on the wing may then be utilized by the take-off model (discussed shortly). Apart from the wing optimization scheme, the lifting-line program may also be used for other wing design aspects, the most important of which being the wing structural analyses.

Figure 12 shows a sample of the lifting-line program output. The top two plots represent the global lift and drag coefficients, used primarily in the optimization scheme. The bottom left plot was used to determine the most aerodynamically efficient angle of attack. Once this was known, the loading distribution along the wingspan due to lift (bottom right plot) was used to easily determine the shear stress and bending moment diagrams shown in *Appendix D*. These plots were to be used in a stress analysis performed after the optimization study, which was critical to wing structural design but beyond the scope of this discussion

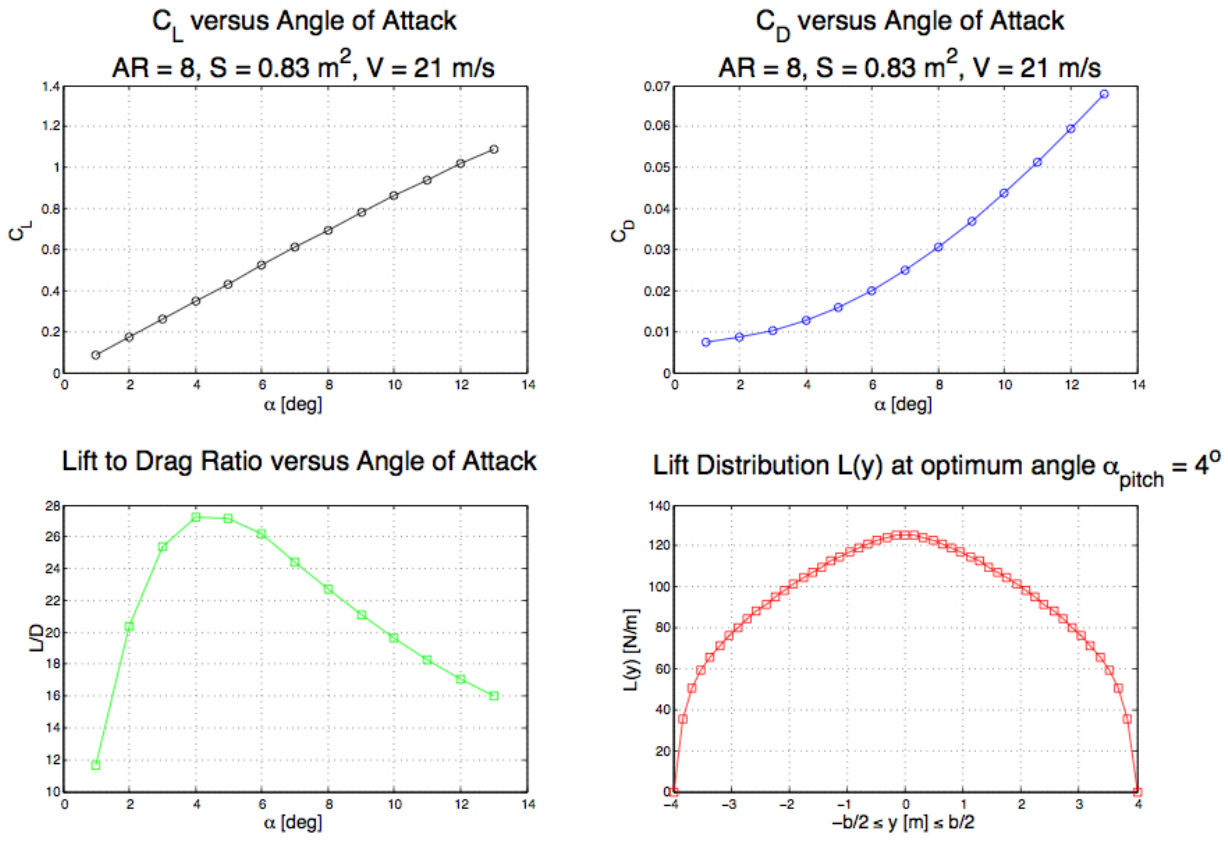

Figure 12: A sample output bundle provided by the lifting-line program.

3 Take-Off Model

3.1 Derivation of Take-Off Equation

The take-off distance requirement of 200 feet was identified to be the limiting criterion in the determination of the maximum allowable payload weight for a given design. Consequentially, a considerable effort was concentrated in the construction of a comprehensive mathematical model (based on *Newtons 2nd Law*) to describe this phase. The concept of the free-body diagram was employed to begin this derivation, which is shown below for this specific case.

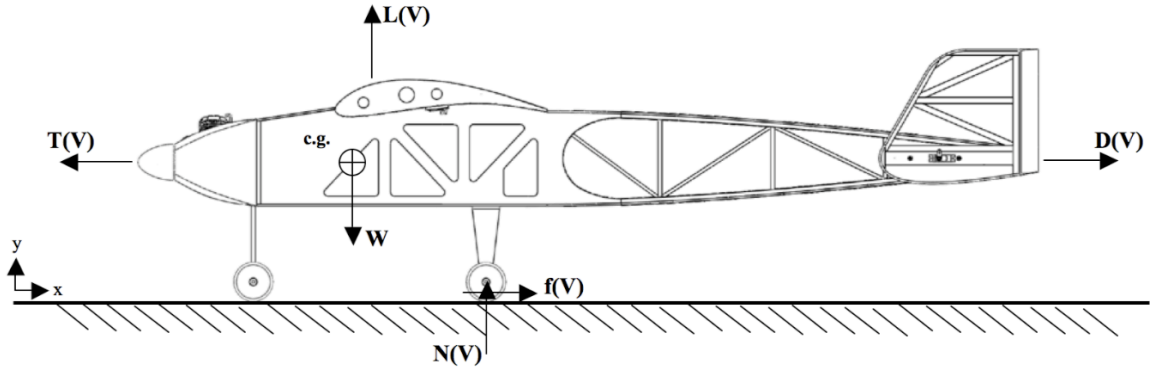

Figure 13: A free body diagram depicting and labeling the forces experience by the aircraft during the take-off phase of operation.

The forces in this free-body diagram are defined and summarized as follows:

- **L(V)** - the lift produced by the main wing. During the take-off, $\alpha_{\text{pitch}} = 0^{\text{o}}$. Therefore the lift coefficient obtained from the aerodynamic model was evaluated at this angle. The standard definition of the lift coefficient was used to express this force as a function of velocity.

$$L(V) = \frac{1}{2}\rho_{\infty}V^2 S C_{\text{L}}(\alpha_{\text{pitch}}) \tag{34}$$

- **D(V)** - the total drag of the aircraft, approximated as the summation of drag contributions from each structural component of the aircraft (*i.e.* fuselage, landing gear, etc.). The equation below represents the summation of the major components considered in a comprehensive drag model[7].

$$D(V) = D_{\text{fuselage}} + D_{\text{wing}} + D_{\text{landing gear}} + \sum D_{\text{tail surfaces}} \tag{35}$$

- **T(V)** - the propulsive thrust function. Given the engine constraint, the selection of the propeller was the only propulsion design parameter allowed by the competition. Wind tunnel testing was ultimately employed for six unique propeller types to determine this function.

[7]The aircraft drag model was developed by multiple members of the design team involving the method proposed by [2]; however, the details of this study expand beyond the scope of this discussion.

- **W** - total aircraft weight. A weight component study initially estimated aircraft weight $W_{\text{AC}} \approx 6$ $[lbs.]$, and may be more exactly set upon completion of the final design. Knowing the maximum value of W will allow for the determination of the maximum payload weight W_{pay} from the following relation.

$$W_{\text{pay}} = W - W_{\text{AC}} \tag{36}$$

- **N(V)** - the normal reaction for exerted by the ground on the aircraft.

- **f(V)** - the rolling friction of the wheels, which can be related to the normal force as follows. The value of μ was approximated to be 0.03 from [7].

$$f(V) = \mu N(V) \tag{37}$$

As can be seen from the free-body diagram, every force acting on the aircraft during take-off (with the exception of the weight parameter) is dependent on velocity. Summing up all the forces with respect to the coordinate axes shown results in the following component equations.

$$\sum F_x : \quad D(V) + f(V) - T(V) = -ma \tag{38}$$
$$\sum F_y : \quad L(V) + N(V) - W = 0 \tag{39}$$

The friction function $f(V)$ can be expressed as a function $L(V)$ and W from substitution of Eq. (39) into Eq. (37).

$$f(V) = \mu \left(W - L(V)\right) \tag{40}$$

Substitution of Eq. (40) into Eq. (38) yields the following relationship.

$$D(V) + \mu \left(W - L(V)\right) - T(V) = -ma \tag{41}$$

The aircraft acceleration may be considered as the second time derivative of displacement. Utilizing the *chain rule* from fundamental calculus, the acceleration may also be expressed as a function of displacement. Replacing the total aircraft mass m with the equivalent weight over gravity W/g, the inertial force may be expressed as follows.

$$ma = \frac{W}{g}\frac{d^2s}{dt^2} = \frac{W}{g}V\frac{dV}{ds} \tag{42}$$

Now Eq. (41) may be expressed as a first-order, nonlinear ordinary differential equation which governs the aircraft velocity as a function of displacement.

$$D(V) - \mu \left(W - L(V)\right) - T(V) = -\frac{W}{g}V\frac{dV}{ds} \tag{43}$$

For this case, the boundary conditions were chosen as follows.

$$s\left(V = 0\right) = 0 \tag{44}$$
$$s\left(V = V_{TO}\right) = S_G \tag{45}$$

This equation may now be solved for the take-off roll distance S_G by the method of *Separation of Variables* from introductory differential equations.

$$S_G = \frac{W}{g} \int_0^{V_{TO}} \frac{V dV}{T(V) - \mu\left(W - L(V)\right) - D(V)} \tag{46}$$

Eq. (46) was modified slightly to account for the aircraft pitch rotation just prior to touching off the ground. The following equation was suggested from Nicolai [7], which assumes that this rotation occurs in an additional 1/3 seconds at V_{TO}.

$$S_{TO} = 200 \text{ [feet]} \approx S_G + \frac{1}{3} V_{TO} \tag{47}$$

Eq. (47) establishes that S_{TO} is dependent on two variables: V_{TO} and W. In order to close this system V_{TO} was approximated as being directly proportional to the stall velocity of the wing V_{stall} by the empirical relationship shown below.

$$V_{TO} \approx 1.2 \; V_{\text{stall}} = 1.2 \sqrt{\frac{2W}{\rho S C_{\text{Lmax}}}} \tag{48}$$

Simplification of the previous discussion results in the final form of the take-off equation.

$$\boxed{S_{TO} = \frac{W}{g} \int_0^{1.2\sqrt{\frac{2W}{\rho S C_{\text{Lmax}}}}} \frac{V dV}{T(V) - \mu\left(W - L(V)\right) - D(V)} + \frac{2}{5} \sqrt{\frac{2W}{\rho S C_{\text{Lmax}}}}} \tag{49}$$

This equation establishes the desired relationship between W and S_{TO}; however, the resulting expression is convoluted. Therefore, solving for W is not a trivial task, requiring a manual iterative-type approach to back out the solution. Recall, that if W is known then the payload weight may be easily found via Eq (36).

3.2 Numerical Implementation of the Take-Off Model

As shown above, the derived expression for the payload weight involves a complicated integrand function with respect to velocity, where each force term (*i.e.* $T(V)$, $D(V)$, etc.) are sub-functions of velocity. While an analytical solution was originally sought, it was eventually decided by the team to resort to numerical techniques. The solution of the take-off equation for W was a collaborative effort by several members of the design team, and as a result, Excel was chosen as the software platform due to its familiarity and general ease of use. The integral representation of S_G was approximated by use of the *trapezoidal rule*.

Figure 14 shows the trend for the distance traveled by the aircraft down the runway corresponding to velocity. The blue curve represents the physical behavior of the aircraft throughout the take-off roll distance phase, where the red curve accounts for the pitch roll phase. This trend was determined by manually adjusting W until S_{TO} was approximately equal to 200 feet. This maximum value of weight corresponds to: (1) the ambient conditions in the form of ρ_{air}, (2) a given wing design, and (3) the accuracy of all the sub-functions. Overall, this model was successfully validated during flight testing.

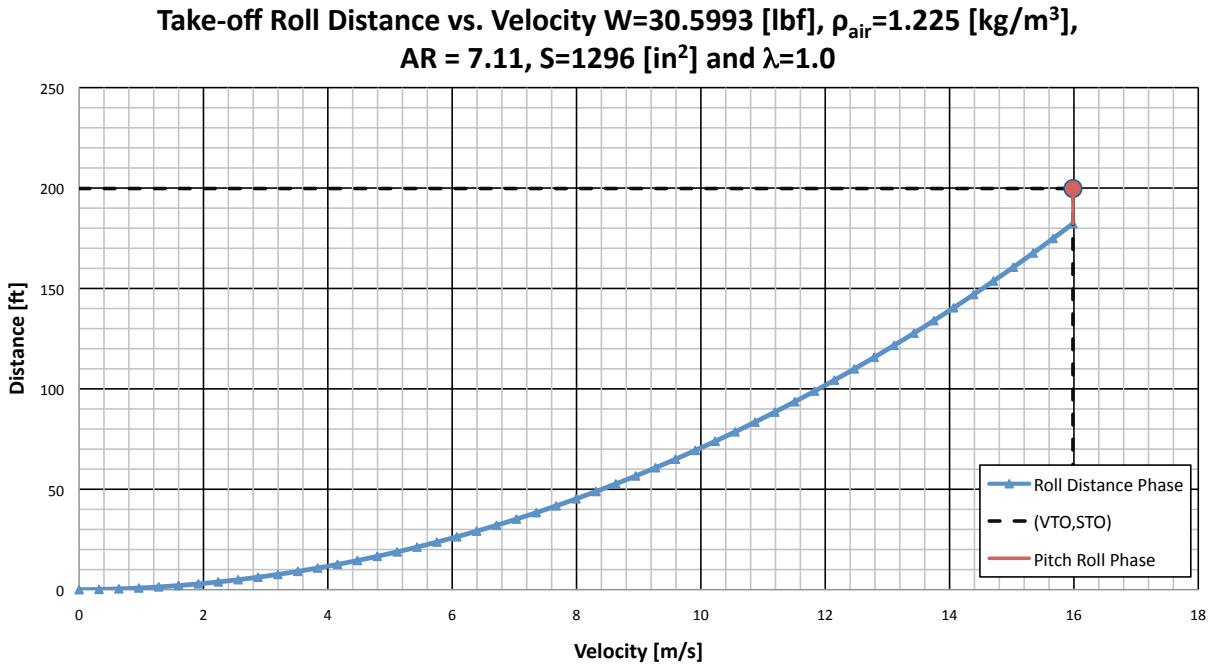

Figure 14: Numerical integral approximation of Eq. (49) used to back out a maximum $W \approx 31[lbf.]$ at standard air density.

4 Wing Optimization Algorithm Results

Upon successful development of the aerodynamic and take-off models, the optimization algorithm discussed in the wing design methodology section 1.2 was employed to determine the overall wing design. The tables and figures below summarize the final design and optimization parameters. It is worth mentioning that both the airfoil profile and taper ratio were ultimately determined in separate studies so as to reduce the design-space to just two variables - wingspan b and chord length c. Both the airfoil selection study and the taper ratio study are further elaborated upon in the Appendices.

Table 1: Summary of the final design parameters for the main wing

Design Parameter	Value	Units
Root chord, c_r	13.5	in
Wingspan, b	96	in
Aspect Ratio, AR	7.11	--
Planform Area, S	1296	in^2
Taper Ratio, λ	1.0	--
Pitch Angle, α	0.0	deg

- **GOE 226 [MAV H,26] profile:**

Table 2: 3-D wing characteristics.

$C_{L(\alpha=0°)}$	0.71
C_{Lmax}	1.574
Stall Angle	≈ 14°

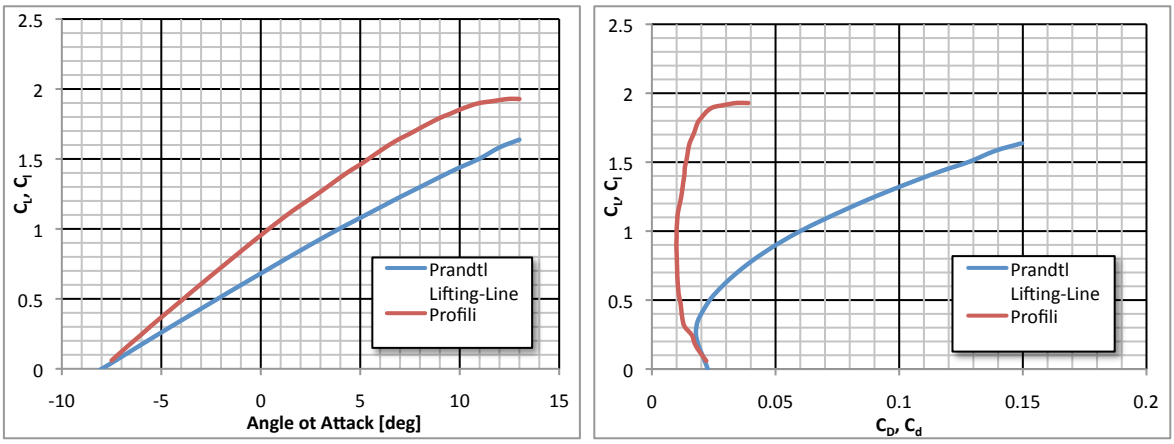

(a) (b)

Figure 15: (a) 2-D and 3-D lift coefficient curves and (b) corresponding lift-drag polars. These trends correspond very closely to the airfoil-to-wing behavior predicted in [8].

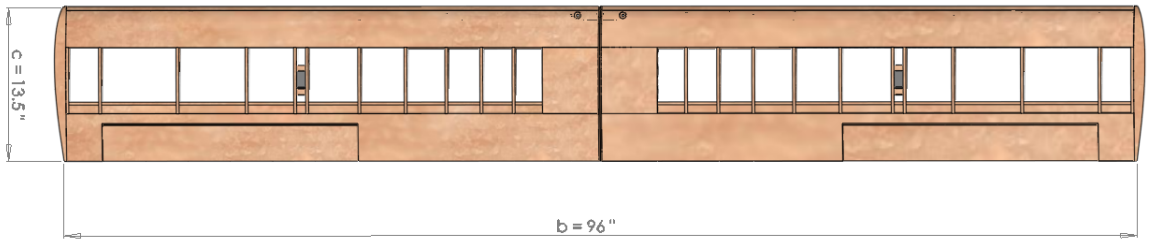

Figure 16: Planform (top) view of the final wing design.

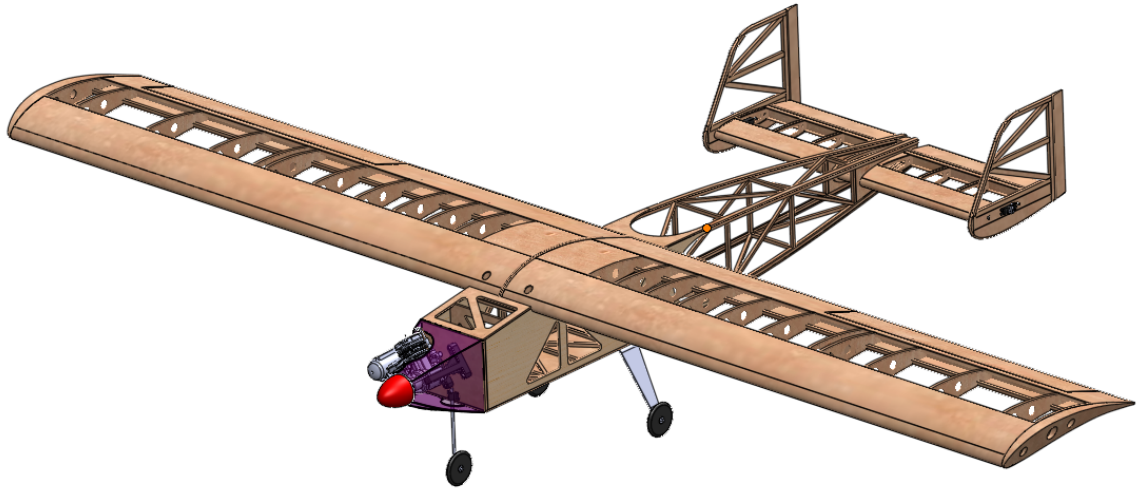

Figure 17: CAD rendering of final aircraft design.

5 Conclusions

The SAE Aero Design® is an international collegiate competition designed to introduce students to real-life engineering challenges in an aerospace related setting. Within this competition, dozens of teams, each comprised of several engineering students under the supervision of one faculty advisor, compete to design, build, and fly a unique remote controlled model aircraft capable of carrying the heaviest payload possible. The competition constraints are designed so as to force each design team to place special focus on aerodynamic optimization, as well as stability/control and structures.

In the case of aerodynamics the main wing of the aircraft was identified as the critical component to be optimized. As such, an optimization algorithm was developed by the team to determined an optimum lifting wing of set dimensions. This algorithm involves two comprehensive analyses: (1) the aerodynamic model and (2) the take-off model. The take-off constraint of $S_{TO} \leq 200$ feet proved to be the limiting criterion with which to ultimately set the wing geometry, and as a result, significant effort was invested in the development of a mathematical model to describe this phase. For the aerodynamic analysis, a classical 3-D wing theory known as *Prandtl's Lifting-Line Theory* was utilized to account for the complicated effects of downwash on finite wings. The optimization scheme resulted in a final wing design that utilizes a GOE 226 [MVA H,26] airfoil profile on a square wing planform with a wingspan of 96 inches and a chord length of 13.5 inches. Most importantly, this wing design is predicted to lift a total weight of 30.5 $[lbf]$ at an air density $\rho_{air} = 1.225$ $[\frac{kg}{m^3}]$.[8]

6 Acknowledgments

A special thanks is deserved to the other four members of the SAE Aero Design LSU Flying Tigers: Edward Scheuermann, Ian Walsdorf, Teddy Bounds, and Eric Bourgeois, as well as to our advisor, Dr. Keith Gonthier. This entire project has been a collaborative effort with which I am privileged to be associated with such talented individuals as the *LSU Flying Tigers*. Finally, the Louisiana Space Consortium, LaSPACE, and Hobby Town USA all played a critical role in supporting this project.

[8]The maximum weight at this density, along with the knowledge that $W = 0$ $[lbf]$ at $\rho_{air} = 0$ $[\frac{kg}{m^3}]$, was used to determined a correlation of how W varies with ρ_{air}. This trend was generated by a separate member of the design team and is beyond the scope of this report.

References

[1] 2009 SAE Aero Design® Rules, http://students.sae.org/competitions/aerodesign/rules/

[2] Corke, Thomas C., *Design of Aircraft*, Upper Saddle River: Pearson Education, Inc., 2003.

[3] Anderson, John D Jr., *Fundamentals of Aerodynamics*, McGraw Hill, Inc., 2007.

[4] Gonthier, Keith A., *Numerical Implementation of a Lifting-Line Method*, ME 4943 Class Handout, Fall 2007.

[5] Drela, Mark, *XFOIL: Subsonic Airfoil Development System*, MarkDrela@mit.edu http://web.mit.edu/drela/Public/web/xfoil/, Feb. 17,2008.

[6] Stefano, Duranti, *Profili 2*, info@profili2.com, http://www.profili2.com/, Copyright 1997-2009.

[7] Nicolai, Leland M., "Estimation R/c Model Aerodynamics and Performance", White pages, 2002.

[8] McCormick, Barnes W., *Aerodynamics, Aeronautics, and Flight Mechanics*, John Wiley & Sons, Inc., 1995.

Appendices

A Lifting-Line Matlab Function

```
function [CL,CD,CDi,CM]  = lift_line_slvr(U,alpha,AR,S)
%John W Dykes
%Senior Design
%Advisor: Dr. Gonthier
%Dr. Wahab
% clear all;
% clf;
% clc;
global N dy A Alphaeff rho chord b
%Import Airfoil Data###########################################################
[A] = fscanf(fopen('GOE 226 [MVA H,36].txt','r'), '%g %g %g %g %g',[5 inf]);
%[A] = fscanf(fopen('MVA-227.txt','r'), '%g %g %g %g %g',[5 inf]);
%[A] = fscanf(fopen('GOE 234 [MVA CA5].txt','r'), '%g %g %g %g %g',[5 inf]);
%###############################################################################
%
%  U = 21*39.37;%in/s
%  alpha = 0;
%  AR = 96/13.5;
%  S = 1296; %in^2
rho=1.12365e-7; %(lbf*s^2)/in^4

% Define parameters and constants##############################################
% initial guess and preleminary constants
N = 100;
taper = 1;
gamma0 = 0;
iterations = 0;
diff = ones(1,N+1);
D = .05;

% Program body#################################################################
b = sqrt(AR*S);
co = (2*b)/(AR*(1+taper));%root chord
dy = b/N;
i = 1;
for j = 1:N+1
    y(j) = -(b/2)+(j-1)*dy;
    c(j) = co*(2*(taper-1)*(abs(y(j))/b)+1);
    % make odd gammas and specify an odd y for plotting
    if (mod(j,2) == 1)
        gamma(j) = gamma0*sqrt(1-(2*y(j)/b)^2);
        Y(i) = y(j);
```

```
        i = i+1;
    end
end

% start convergence loop
while (norm(diff) > 1e-8)
    i = 1;
    iterations = iterations+1;
    diff = zeros(1,N+1);
    for j = 1:2:(N+1)
        gammaold(j) = gamma(j);

        % define integrand
        for k = 2:2:N
            dgdy(k) = (gamma(k+1)-gamma(k-1))/(2*dy);
            F(k) = dgdy(k)/(y(j)-y(k));
        end

        sumk(j) = F(2)+F(N)+2*sum(F(4:(N-2)));
        sumk(j) = dy*sumk(j)+.5*dy*(.5*(3*F(2)-F(4))+F(2)+F(N)+.5*(3*F(N)-F(N-2)));

        % find alpha values
        alphai(j) = sumk(j)/(4*pi*U);
        alphaeff(j) = (alpha*(pi/180)-alphai(j))*(180/pi);

        %find cl and cd for imputed airfoil
        cl(j) = spline(A(1,:),A(2,:),alphaeff(j));

        % compute new gamma
        gammanew(j) = .5*U*c(j)*cl(j);

        % reset gamma and define convergence criterion
        if (j~=1 && j~=(N+1))
            gamma(j) = gammaold(j)+D*(gammanew(j)-gammaold(j));
            diff(j) = abs(gamma(j)-gammaold(j));
        else
            gamma(j) = 0;
        end

        %redifine matricies for plot commands
        Alphai(i) = alphai(j)*(180/pi);
        Alphaeff(i) = alphaeff(j);
        i = i+1;
    end
    %dangerous extrapolation on wing tips
    Alphai(1) = Alphai(2)+Alphai(3)-Alphai(4);
    Alphaeff(1) = Alphaeff(2)+Alphaeff(3)-Alphaeff(4);
```

```
    Alphai(N/2+1) = Alphai(N/2)+Alphai(N/2-1)-Alphai(N/2-2);
    Alphaeff(N/2+1) = Alphaeff(N/2)+Alphaeff(N/2-1)-Alphaeff(N/2-2);
end
i = 1;
for j = 1:2:(N+1)
    gammasin(j) = gamma(j)*sin(alphai(j));
    gammacos(j) = gamma(j)*cos(Alphai(i)*pi/180);
    cdo(i) = spline(A(1,:),A(3,:),Alphaeff(i));
    chord(i) = c(j);
    Gamma(i) = gamma(j);
    lift(i) = rho*U*Gamma(i)*cos(Alphai(i)*pi/180);
    dragi(i) = lift(i)*tan(Alphai(i)*pi/180);
    drago(i) = .5*rho*U^2*c(j)*cdo(i);
    drag(i) = dragi(i) + drago(i);
    i = i+1;
end

% get CL, CD, LDiratio
CL = 2*dy/(U*b*(c(1)+c(N/2+1))/2)*(gammacos(1)+gammacos(N+1)+2*sum(gammacos(3:N-1)));
CD = 2*dy*(drag(1)+drag(N/2+1)+2*sum(drag(2:N/2-1)))/(.5*rho*U^2*b*(c(1)+c(N/2+1)));
CDi = 2*dy*(dragi(1)+dragi(N/2+1)+2*sum(dragi(2:N/2-1)))/(.5*rho*U^2*b*(c(1)+c(N/2+1)));

% get bending moments and torque about AC.###################################
[Moments] = moment_slvr(Y,alpha,lift,drag,U);
CM = Moments(1,5)/(.5*rho*U^2*S*chord(N/4+1));
% get moment of inertias#####################################################
[Inertias] = inertia_calc(Y,chord);
% get max bending stresses over the halfspan#################################
[y_crit] = stress_func(Moments,Inertias);

%plot some results##########################################################
.
.
.
```

B Airfoil Selection Study

The airfoil for the main wing was selected prior to the determination of the other wing design parameters. This selection was performed using the initial aircraft design spreadsheet values [2] and involved a decision-matrix-type weighted table, evaluated at a fixed aircraft weight of 30 [$lbs.$]. These constant parameters were only set to establish a definitive relationship with which to evaluate the airfoil profiles with respect to each other and, thus, were only guesses at this point for the final wing planform shape and payload weight. The initial study involved a selection of 30 airfoil profiles that were subjectively different in profile from each other. A second study was then done after a certain high-chambered feature was identified as optimal from the first study. The airfoils were judged on three criterions and weighted as follows: (1) the take-off distance $\sim$50%, (2) the cruise velocity $\sim$20%, and (3) the stall margin $\sim$30%. For these studies, the airfoil profiles were awarded points for obtaining (i) the shortest take-off distance (corresponding to the highest weight to potentially take-off), (ii) the lowest cruise velocity (corresponding to the most aerodynamically efficient wing with the lowest lift-to-drag ratio), and (iii) the stall margin (corresponding to the most forgiving stall properties). The selected airfoil for the main wing was the **GOE 226 [MVA H,36]**.

C Taper Ratio Study Results

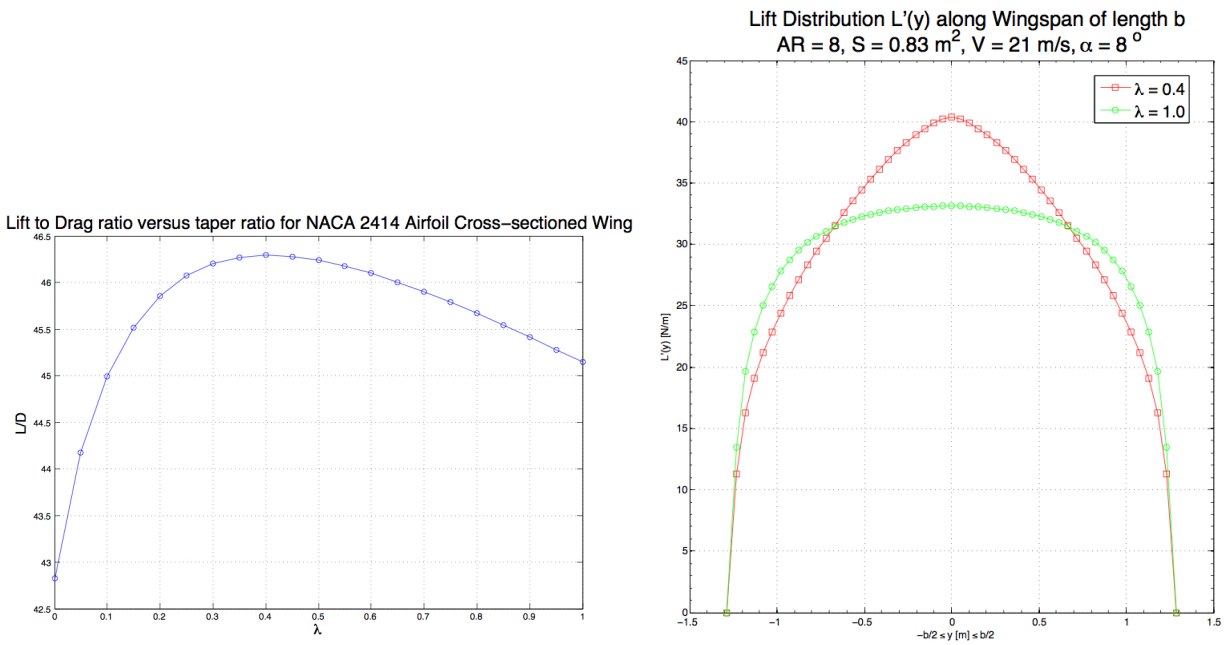

(a) (b)

Figure 18: (a) The taper ratio study confirmed $\lambda = 0.4$ to be the optimum value for a wing of constant S and AR as claimed by [8]; however, $\lambda = 1.0$ was chosen for the final design to maximize S, and (b) comparison between lift distributions for the untapered and optimum tapered cases.

D Aerodynamic & Bending Moment Sample Output File

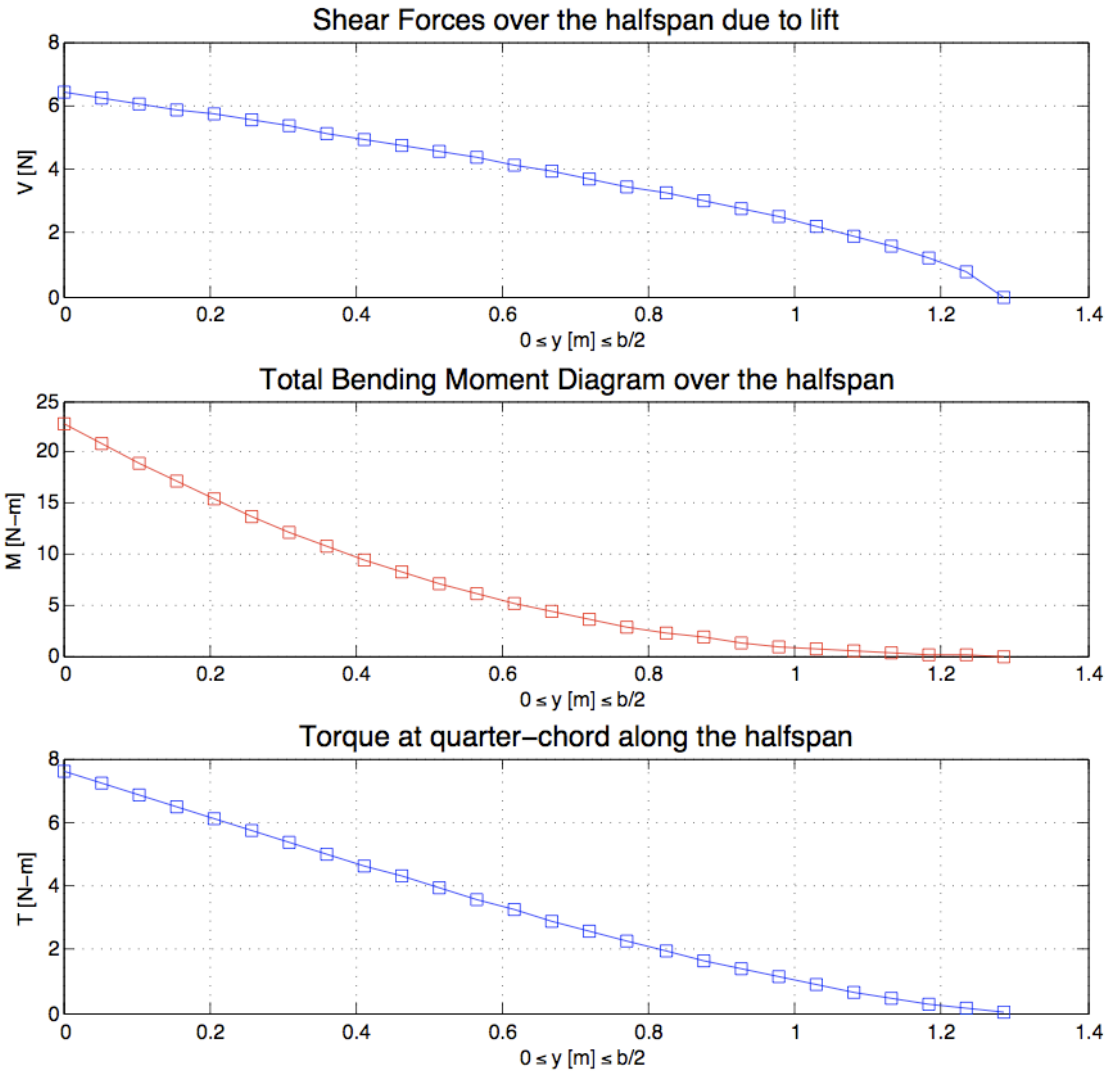

Figure 19: For the stress analyses, this information helped streamline bending stress and Euler Buckling studies; for the stability the torque was integrated and used to set the longitudinal stability.